

Mechanistic Organic Chemistry in a Microreactor. Zeolite-Controlled Photooxidations of Organic Sulfides

Edward L. Clennan,* Wenhui Zhou, and Jacqueline Chan

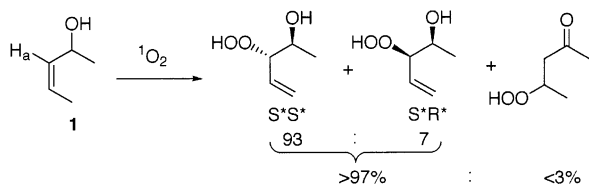
Department of Chemistry, University of Wyoming, Laramie, Wyoming 82071

Clennane@uwyo.edu

Received July 10, 2002

The intrazeolite and solution photooxygenations of a series of sulfides have been compared. The unusual zeolite environment enhances the rates of reaction, it suppresses the Pummerer rearrangements, and it has a dramatic effect on the sulfoxide/sulfone ratio. A detailed kinetic study utilizing trapping experiments and intramolecular competition provides evidence for cation complexation to a persulfoxide intermediate as the underlying phenomenon for the unique intrazeolite behavior. For example, the enhanced rate of reaction is traced to the cation stabilization of the persulfoxide toward unproductive decomposition to substrate and triplet oxygen.

Remarkable progress in the control of regio- and stereoselectivity in organic transformations has been achieved in the past 25 years.¹ However, the further development of new methodology to control the introduction of stereogenic elements is essential in order to devise economically efficient syntheses of complex organic molecules. A fundamental feature of many successful regio- and/or stereoselective synthetic strategies is the simultaneous control of the conformational flexibility and of the approach geometry of the reacting components. Synthetically useful levels of control utilizing this feature have been achieved by either careful reaction component design or by the use of supramolecular systems to impart “enzyme-like” organization to the substrates and activated complexes.² For example, Adam and co-workers,^{3–5} have used the reaction component design approach to cleverly couple allylic strain ($A_{1,3}$ strain) with hydrogen-bonding effects to control both the conformation of allylic alcohol **1** and the direction of singlet oxygen attack to give stereoselectively the S^*S^* diastereomer.



The supramolecular approach has also been extensively utilized. For example, several groups^{6–13} have used

zeolites as supramolecular hosts to influence the regio-chemistry and stereochemistry¹⁴ of the singlet oxygen ene reaction. Despite the advantages of this supramolecular/zeolite approach, rationale implementation is impeded by the paucity of information on how the zeolite environment can influence reaction mechanisms. To help rectify this situation, we describe here a mechanistic study of the reactions of singlet oxygen with organic sulfides in the interior of zeolite Y.¹⁵

Zeolites are crystalline solids consisting of catenated silicon and aluminum tetrahedra that enclose regular repeating cavities or channels of well-defined size and shape. Zeolite Y (NaY) is a member of the faujasite family with a typical unit cell composition of $Na_{56}(AlO_2)_{56}(SiO_2)_{136} \cdot 264H_2O$.¹⁶ It is characterized by a honeycomb structure consisting of eight supercages per unit cell each approximately 13 Å in diameter and each accessible through tetrahedrally arranged windows approximately 7.4 Å in diameter (Scheme 1). The supercages of zeolite Y are electrostatically charged as a result of seven counterions that balance the negative charges on the tetravalent framework aluminum atoms.

(7) Robbins, R. J.; Ramamurthy, V. *J. Chem. Soc. Chem. Commun.* **1997**, 1071–1072.

(8) Shailaja, J.; Sivaguru, J.; Robbins, R. J.; Ramamurthy, V.; Sunoj, R. B.; Chandrasekhar, J. *Tetrahedron* **2000**, *56*, 6927–6943.

(9) Stratakis, M.; Froudakis, G. *Org. Lett.* **2000**, *2*, 1369–1372.

(10) Stratakis, M.; Rabalakos, C. *Tetrahedron Lett.* **2001**, *42*, 4545–4547.

(11) Stratakis, M.; Kosmas, G. *Tetrahedron Lett.* **2001**, *42*, 6007–6009.

(12) Clennan, E. L.; Sram, J. P. *Tetrahedron Lett.* **1999**, *40*, 5275–5278.

(13) Clennan, E. L.; Sram, J. P. *Tetrahedron* **2000**, *56*, 6945–6950.

(14) Joy, A.; Robbins, R. J.; Pitchumani, K.; Ramamurthy, V. *Tetrahedron Lett.* **1997**, *38*, 8825–8828.

(15) For a preliminary account of this research, see: Zhou, W.; Clennan, E. L. *J. Chem. Soc. Chem. Commun.* **1999**, 2261–2262m. Zhou, W.; Clennan, E. L. *Org. Lett.* **2000**, *2*, 437–440. Zhou, W.; Clennan, E. L. *J. Am. Chem. Soc.* **1999**, *121*, 2915–2916.

(16) Ramamurthy, V.; Garcia-Garibay, M. A. In *Solid-State Supramolecular Chemistry: Two- and Three-Dimensional Inorganic Networks*; Alberti, G., Bein, T., Eds.; Elsevier Science Ltd.: Tarrytown, New York, 1996; Vol. 7, pp 693–719.

* Corresponding author. Fax: 307-766-2807.

(1) Eliel, E. L.; Wilen, S. H. *Stereochemistry of Organic Compounds*; John Wiley & Sons: New York, 1994; Chapter 12, pp 835–990.

(2) Clennan, E. L. *Tetrahedron* **2000**, *56*, 9151–9179.

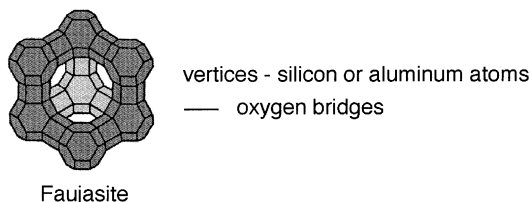
(3) Adam, W.; Nestler, B. *J. Am. Chem. Soc.* **1992**, *114*, 6549–6550.

(4) Adam, W.; Nestler, B. *J. Am. Chem. Soc.* **1993**, *115*, 5041–5049.

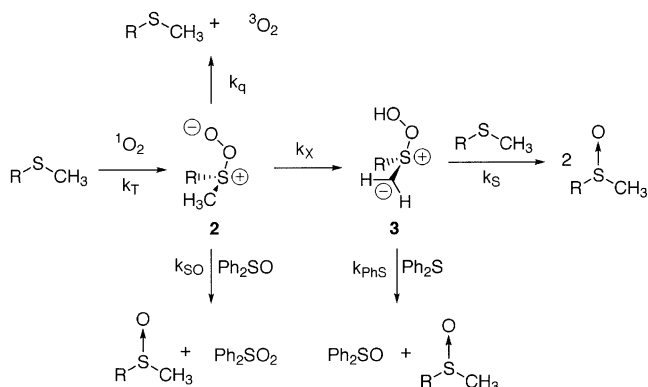
(5) Adam, W.; Gevert, O.; Klug, P. *Tetrahedron Lett.* **1994**, *35*, 1681–1684.

(6) Li, X.; Ramamurthy, V. *J. Am. Chem. Soc.* **1996**, *118*, 10666–10667.

SCHEME 1



SCHEME 2. A Generic Mechanism for the Reaction of Singlet Oxygen with Sulfides in Aprotic Solvents



The sulfide singlet oxygen system was chosen for our initial investigations since dialkyl and aryl sulfide photooxidations are expected to be dramatically affected by the extraordinary environment found in the interior of zeolite Y. This expectation is a direct result of extensive studies over the past 20 years that have culminated in a mechanistic suggestion (Scheme 2) that invokes two charge-separated intermediates, the persulfoxide **2** and the hydroperoxysulfonium ylide **3**, on the potential energy surface.^{17–19}

The addition of $^1\text{O}_2$ to the sulfide occurs on a very flat potential energy surface to give persulfoxide **2** as the first stationary point. It is the decomposition of this intermediate along a physical quenching pathway, k_q , that is responsible for the very low experimentally observed quantum yields ($\Phi < 0.05$) in these reactions. The persulfoxide **2**, in competition with physical quenching, also undergoes a very novel intramolecular hydrogen abstraction from the α -carbon to give the second observed stationary point on the reaction surface, the hydroperoxysulfonium ylide **3**. This second intermediate then reacts with the sulfide substrate to give two molecules of sulfoxide. Not depicted in Scheme 2 are two very interesting rearrangements of **3** that have been observed as competing processes with some substrates: (1) a 1,2-shift of the hydroperoxy group (OOH) to the anionic α -carbon in a Pummerer-like rearrangement to ultimately give S–C bond cleavage products^{20–23} and (2) a

1,2-shift of the hydroxy group (OH) from oxygen to sulfur to ultimately give sulfone.²⁴

Experimental evidence that supports the solution-phase mechanism depicted in Scheme 2 includes (1) formation of Ph_2SO_2 during cophotooxidations with Ph_2SO , which is itself inert to singlet oxygen (k_{SO} in Scheme 2); (2) formation of Ph_2SO during cophotooxidations with Ph_2S , which is also inert to singlet oxygen (k_{PhS} in Scheme 2); (3) the kinetic demonstration that Ph_2S but not Ph_2SO competes with the sulfide substrate for a reaction intermediate; (4) the kinetic demonstration that Ph_2SO but not Ph_2S increases the quantum yield of the reaction by competing with physical quenching, k_q ; (5) the use of substituted diaryl sulfide and sulfoxide trapping agents, which demonstrate that the first intermediate is nucleophilic and the second intermediate is electrophilic; and (6) product isotope effects, which require the removal of an α -hydrogen on the reaction surface for formation of the sulfoxide product. Our experimental approach in this study was to first survey the intrazeolite photooxidations of a variety of sulfide structural types (e.g. dialkylsulfides, cyclic sulfides, acyclic sulfides, and aryl sulfides) and then to focus on a mechanistic examination of one of the sulfide substrates. The results from this experimental approach are described below.

Results

Product Studies. The homogeneous (solution) and heterogeneous (intrazeolite) photooxidations of 11 sulfides have been examined. A comparison of the results in the two media and the details of the intrazeolite photooxidations are given in Figure 1 and Table 1, respectively.

The intrazeolite photooxidations were conducted by irradiations of oxygen-saturated hexane slurries containing the sulfide substrate and methylene blue-doped NaY with a 600-W tungsten–halogen lamp through a 400-nm cutoff filter (saturated NaNO_2). The methylene blue-doped zeolite (NaMBY) was prepared by adding NaY to an aqueous solution of methylene blue and stirring until the blue color of the water completely faded and the zeolite powder turned blue. The NaMBY was then filtered and dried at $100\text{ }^\circ\text{C}$ at 10^{-4} Torr for 24 h. The loading level of methylene blue was on average one molecule per every 100 supercages ($\langle S \rangle = 0.01$) or 15 molecules per every 10 000 supercages ($\langle S \rangle = 0.0015$). In most of the work, the higher loading level was used, since sensitizer bleaching was a minor annoyance at the lower loading level. The reactions were worked up by filtration followed by mild digestion of the zeolite with 10% aqueous HCl and extraction with acetonitrile, tetrahydrofuran, or chloroform. The percent recovery with this workup protocol was in excess of 95%, except where noted (Table 1).

Gas chromatographic monitoring of the hexane component of the slurries demonstrated that migration of the sulfides into the interior of the zeolite was nearly

(17) Jensen, F.; Greer, A.; Clennan, E. L. *J. Am. Chem. Soc.* **1998**, *120*, 4439–4449.

(18) Touthkine, A.; Clennan, E. L. *J. Org. Chem.* **1999**, *64*, 5620–5625.

(19) Touthkine, A.; Clennan, E. L. *Tetrahedron Lett.* **1999**, *40*, 6519–6522.

(20) Takata, T.; Hoshino, K.; Takeuchi, E.; Tamura, Y.; Ando, W. *Tetrahedron Lett.* **1984**, *25*, 4767–4770.

(21) Takata, T.; Tamura, Y.; Ando, W. *Tetrahedron* **1985**, *41*, 2133–2137.

(22) Takata, T.; Ishibashi, K.; Ando, W. *Tetrahedron Lett.* **1985**, *26*, 4609–4612.

(23) Clennan, E. L.; Aebisher, D. *J. Org. Chem.* **2002**, *67*, 1036–1037.

(24) Ishiguro, K.; Hayashi, M.; Sawaki, Y. *J. Am. Chem. Soc.* **1996**, *118*, 7265–7271.

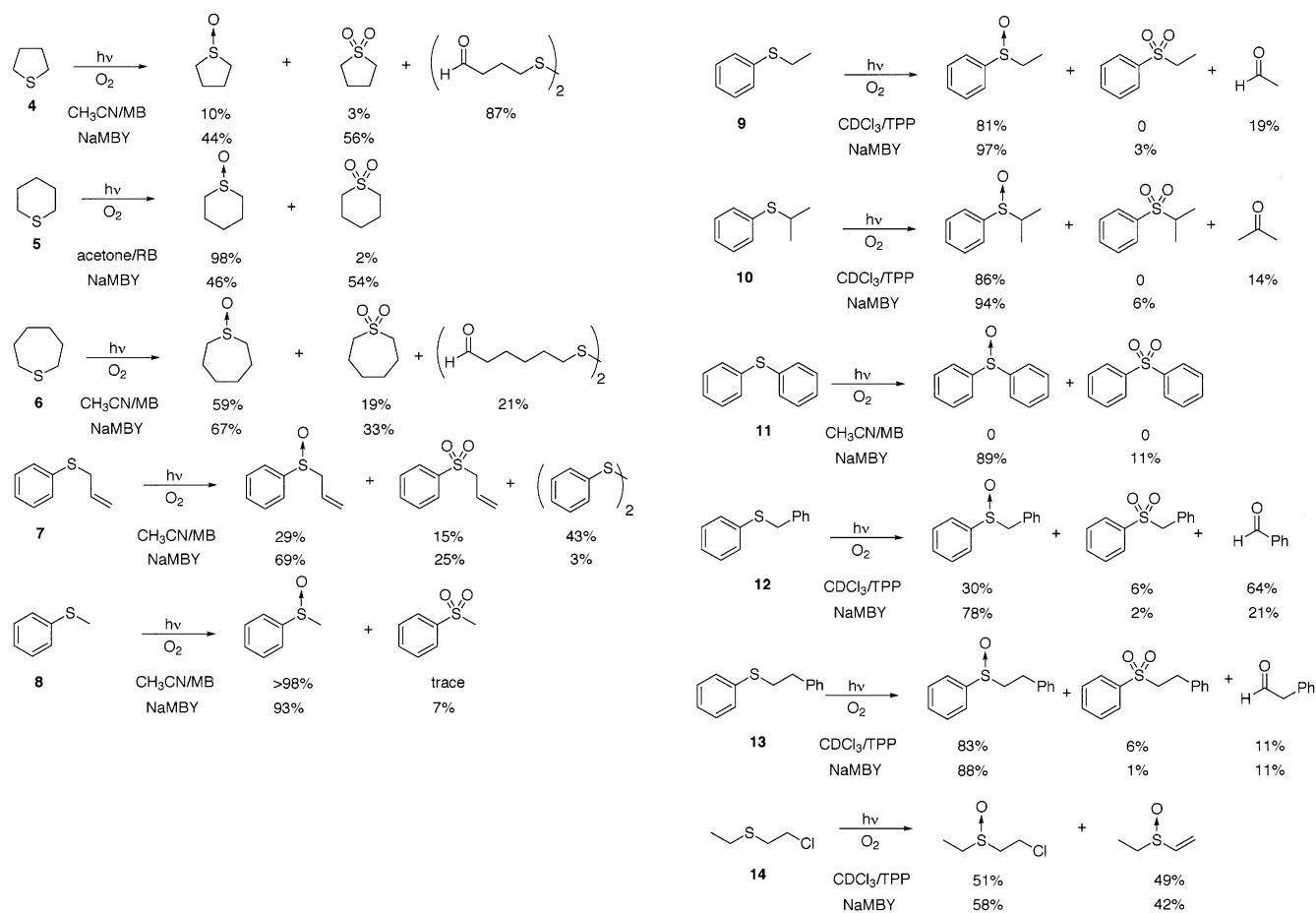


FIGURE 1. A Comparison of the solution and intrazeolite photooxidations of sulfides 4–14.

TABLE 1. Intrazeolite Photooxidations of Sulfides 4–14^a

| sulfide | $\langle S \rangle_{MB}^b$ | $\langle S \rangle_S^c$ | $h\nu$ time | % convn | % SO ^{d,f} | % SO ₂ ^{e,f} | % cleavage |
|---------|----------------------------|-------------------------|-------------|---------|---------------------|----------------------------------|------------|
| 4 | 0.01 | 0.23 | 1 h | 100 | 44 | 56 | |
| 5 | 0.0015 | 0.26 | 1 h | 100 | 46 | 54 | |
| 6 | 0.01 | 1.06 | 1 h | 100 | 67 | 33 | |
| 7 | 0.01 | 1.06 | 1 h | 100 | 69 | 25 | 3 |
| 8 | 0.01 | 1.3 | 1 h | 46.5 | 93 | 7 | |
| 9 | 0.01 | 1.3 | 1 h | 70.7 | 97 | 3 | |
| 10 | 0.01 | 1.3 | 1 h | 89 | 94 | 6 | |
| 11 | 0.01 | 0.26 | 1 h | 98.7 | 89 | 11 | |
| 12 | 0.01 | 1.3 | 1 h | 35.5 | 78 | 2 | 21 |
| 13 | 0.01 | 1.3 | 1 h | 36.2 | 88 | 1 | 11 |
| 14 | 0.01 | 1.3 | 30 min | 100 | 58 | 42 | |

^a Conducted in a hexane slurry as described in the Experimental Section. ^b Number of methylene blue sensitizers per supercage. ^c Number of substrate molecules per supercage. ^d Sulfoxide. ^e Sulfone. ^f See Figure 1 for structures of substrates and products.

quantitative (>96–98%), even at the highest loading levels ($\langle S \rangle = 1.3$ sulfide molecules per supercage) utilized in this study. Such high loading levels were not feasible in all solvents. For example, a plot (Figure 2) of the number of millimoles (T) of sulfide 5 in the interior of the zeolite versus equilibration time for both hexane and acetonitrile demonstrates that quantitative migration (>98%) into the zeolite to give a loading level of $\langle S \rangle = 1.4$ occurred within 2 min in hexane. In contrast, even after extended periods of time in the acetonitrile slurries, the majority of 5 resided in solution rather than in the

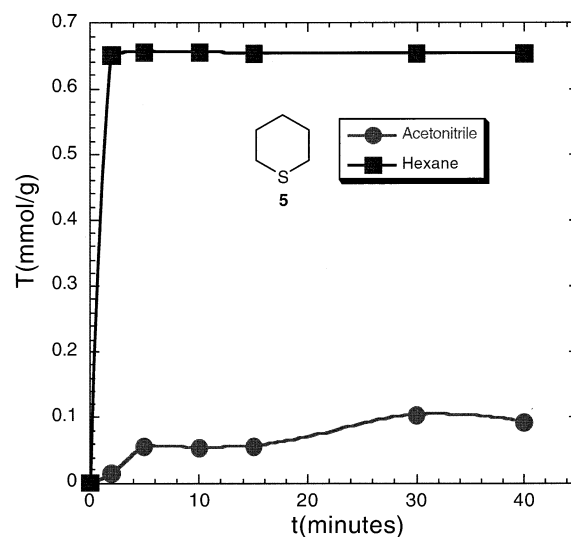


FIGURE 2. Absorption profile for migration of sulfide 5 into NaMBY ($\langle S \rangle_{MB} = 0.01$) in CH₃CN and hexane.

interior of the zeolite. Consequently, hexane was used in all the studies described in this paper.

Under these carefully controlled hexane slurry reaction conditions, interactions between singlet oxygen and the sulfides occur exclusively in the interior of the zeolite. This was established by a series of quenching experiments with the quenchers β -carotene and 2,3-dimethyl-

2-butene and the substrate diphenyl sulfide, **11**. β -Carotene ($k_q = 1.4 \times 10^{10} \text{ M}^{-1} \text{ s}^{-1}$),²⁵ which is too large to migrate into the zeolite, has no effect on the percent conversion of **11**; however, 2,3-dimethyl-2-butene, which can migrate into the zeolite, competitively inhibits the reaction of **11** (see plots S1 and S2 of the Supporting Information).

A comparison of the results from the homogeneous and heterogeneous photooxidations (Figure 1) reveals several unusual features: (1) the yields of sulfone were enhanced by moving the photooxidations into the zeolite, (2) sulfur-carbon bond cleavages via the Pummerer reaction were dramatically suppressed during intrazeolite photooxidations of **4**, **6**, **7**, **9**, **10**, and **12**, and (3) diphenyl sulfide, **11**, was completely inert in solution but reacted nearly quantitatively within 1 h in the zeolite. In fact, most of the intrazeolite reactions occurred more rapidly than their solution counterparts. This reactivity difference was especially evident for the aryl-substituted sulfides.

Mechanistic Studies. As a direct result of the dramatic reactivity enhancement observed for the intrazeolite photooxidation of diphenyl sulfide, **11**, we have focused much of our initial mechanistic work on this compound. However, in a select number of experiments, we have used thiane, **5**, as a representative for dialkyl sulfides to compare to the results obtained with **11**. For example, we have examined the effect of substrate loading level on product composition during the intrazeolite photooxidation of **5** and compared it to the results obtained with **11**. In both cases a linear increase (Figure 3) in the sulfoxide/sulfone ratio was observed as a function of increasing loading level, $\langle S \rangle$. (See Tables S1 and S2 of the Supporting Information for the raw data used to generate Figure 3.) The sensitivity of the sulfoxide/sulfone ratio on $\langle S \rangle$ was approximately 2.3 times greater for **11** than **5**, reflecting the smaller amount of sulfone formed in the **11** intrazeolite photooxidation at low concentrations and perhaps the larger molecular volume of Ph_2S , **11** (236.4 \AA^3), in comparison to thiane, **5** (148.4 \AA^3).²⁶ This effect of substrate concentration is unprecedented in solution, where little or no effect is observed on the sulfoxide/sulfone ratios over a fairly large substrate concentration range.^{27,28}

The sulfoxide/sulfone ratio was also a sensitive function of the degree of hydration of the zeolite. This phenomenon is illustrated for **5** in Table 2, where it is compared to the effect of water on the sulfoxide/sulfone ratio in solution. When the zeolite was air-dried at atmospheric pressure for 24 h, no photooxidation of **5** was observed, even after 1 h of irradiation. Ramamurthy and co-workers²⁹ have previously reported that water promotes the formation of thiazine dye dimers in NaY. The formation of dimers in our 24 h air-dried NaMBY sample was readily confirmed by comparison of solution and diffuse reflectance UV-vis spectra, which demonstrated

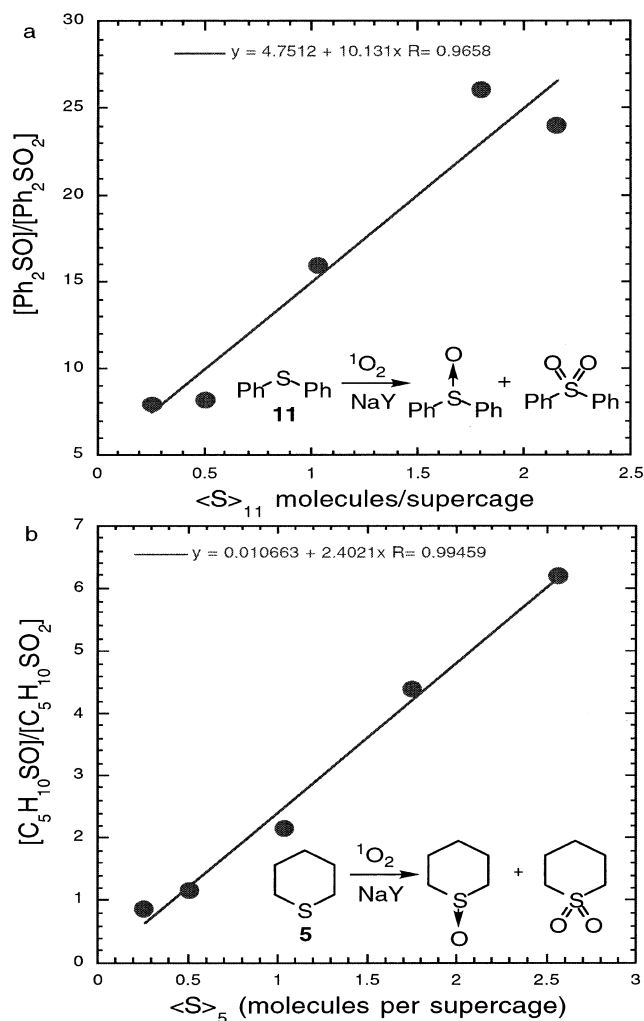


FIGURE 3. The sulfoxide/sulfone product ratio as a function of Ph_2S (**11**, plot a) and thiane (**5**, plot b) loading levels.

TABLE 2. Effect of Water on the Intrazeolite and Solution Photooxidations of **5**

| drying time/[H ₂ O], mol/L | % conversion | % 5-SO ^a | % 5-SO ₂ ^b |
|--|--------------|---------------------|----------------------------------|
| zeolite (1 h <i>hν</i>) ^c | | | |
| 24 h (rt, 1 atm) | no reaction | | |
| 1 h ^e | 78.5 | 27.8 | 72.2 |
| 2 h ^e | 72.2 | 60.5 | 39.5 |
| 8 h ^e | 77.6 | 81.5 | 18.5 |
| solution (1 h <i>hν</i>) ^d | | | |
| 0 | 100 | 93.6 | 6.4 |
| 0.05 | 100 | 96.5 | 3.5 |
| 0.1 | 100 | 95.7 | 4.3 |
| 0.5 | 100 | 96.2 | 3.8 |
| 1.0 | 100 | 89.4 | 10.6 |
| 5.0 | 100 | 100 | trace |

^a Thiane sulfoxide. ^b Thiane sulfone. ^c In hexane slurry containing 1% ($\langle S \rangle_{\text{MB}} = 0.01$) NaMBY. ^d In acetonitrile containing $6 \times 10^{-4} \text{ M MB}$. ^e At 100 °C and $6 \times 10^{-4} \text{ Torr}$.

a dramatic 69-nm hypsochromic shift of λ_{MAX} from 672 nm in solution to 603 nm in NaY. The absence of reaction promoted by this dimeric $\text{Na}(\text{MB})_2\text{Y}$ is consistent with preferential self-quenching rather than singlet oxygen formation. However, drying of the NaMBY sample at 100 °C and $6 \times 10^{-4} \text{ Torr}$ for as little as 1 h resulted in rapid photooxidation. The efficiency of the photooxidation, as

(25) Wilkinson, F.; Helman, W. P.; Ross, A. B. *J. Phys. Chem. Ref. Data* **1995**, *24*, 663–1021.

(26) PC Model, Serena Software, Box 3076, Bloomington, IN 47402-3076.

(27) Clennan, E. L. In *Advances in Oxygenated Processes*; Baumstark, A. L., Ed.; JAI Press: Greenwich, CT, 1995; Vol. IV, pp 49–80.

(28) Clennan, E. L. *Sulfur Rep.* **1996**, *19*, 171–214.

(29) Ramamurthy, V.; Sanderson, D. R.; Eaton, D. F. *J. Am. Chem. Soc.* **1993**, *115*, 10438–10439.

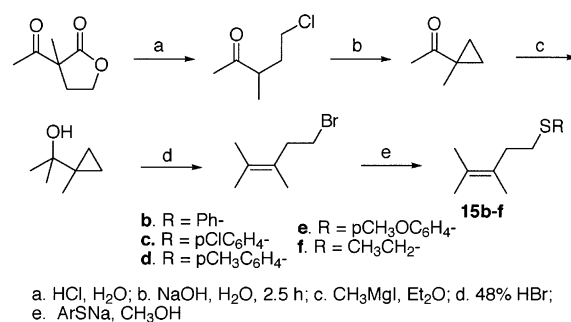
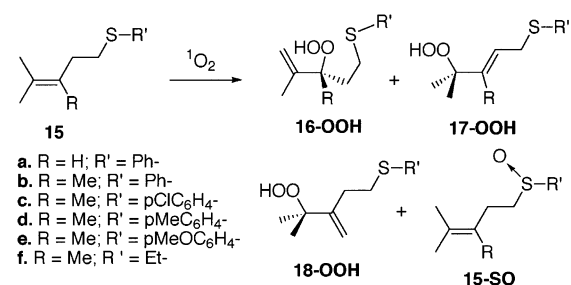
TABLE 3. Photooxidations of 11 as a Function of Cation-Exchanged Zeolite^a

| zeolite | % conversion | [11-SO]/[11-SO ₂] |
|---------|--------------|-------------------------------|
| NaMBY | 95.8 | 89.1/10.9 |
| LiMBY | 95.2 | 91.6/8.4 |
| KMBY | 38.3 | 95.2/4.8 |
| RbMBY | 4.8 | 100/0 |
| CsMBY | 0.5 | 100/0 |
| BaMBY | 50.8 | 98.6/1.4 |

^a Photooxidations conducted with MB loading levels of $\langle S \rangle = 0.01$ in 5-mL hexane slurries for 1 h. The concentrations of **11** in the 5-mL hexane samples were all 0.02 M prior to the addition of the cation-exchanged zeolite.

revealed by percent conversion, was independent of drying time (from 1 to 8 h), but the amount of sulfone dramatically decreased from 72.2% to 18.5% as the water content decreased (Table 2). The diffuse reflectance spectra also revealed a bathochromic shift of λ_{MAX} from 603 nm to a near solution-like λ_{MAX} of 676 nm after the 1 h drying period. No additional shift in λ_{MAX} was observed, even after 8 h of drying under vacuum at 100 °C. In dramatic contrast, little or no change was observed in the sulfoxide/sulfone ratio in acetonitrile over a wide range of water concentrations (Table 2).

The influence of the intrazeolite charge-balancing counterion was explored with a series of ion-exchanged zeolites. The zeolite framework atoms are ineffective at providing extensive shielding from the high electrostatic fields surrounding the cations.³⁰ Consequently, these electrostatic fields can play large roles in the stabilization of charge-separated intermediates.^{30–47} These electrostatic fields, which are typically on the order of 1 to 10 V nm⁻¹ decrease in the order BaY > LiY > NaY > KY > RbY > CsY.³⁰ The data in Table 3 reveal a dramatic electrostatic field effect during the intrazeolite photooxidation of **11** on the percent conversions but only a minor effect on the sulfoxide/sulfone ratio. The low percent conversion in BaY in comparison to LiY or NaY, despite the higher electrostatic field generated by Ba²⁺, reflects

**FIGURE 4.****FIGURE 5.**

the dichotomy between the size of Ba²⁺, which decreases the supercage free volume, and the influence of the electrostatic field.

The dramatic change in the intrazeolite % conversions of **11** depicted in Table 3 can be attributed to either electrostatic-field-induced enhancement of the rate of persulfide (Ph₂S⁺OO⁻) formation or to electrostatic-field-induced stabilization of the persulfide, leading to a decrease in physical quenching (i.e. Ph₂S⁺OO⁻ → Ph₂S + ³O₂). To distinguish between these two possibilities and to develop a greater understanding of intrazeolite sulfide dynamics, we have examined the intrazeolite photooxidations of a series of aryl sulfides, **15a–f** (Figure 5), which are tethered to alkene linkages.⁴⁸ Sulfide **15a**, 2-methyl-5-phenylthio-2-pentene, was synthesized by treatment of 5-bromo-2-methyl-2-pentene⁴⁹ with sodium phenylthiolate. Sulfides **15b–f** were synthesized by treatment of 5-bromo-2,3-dimethyl-2-pentene with the corresponding thiolate as shown in Figure 4.

The photooxidations of sulfides **15a–f** were examined both in solution and in zeolite Y. The electron-rich tetrasubstituted-alkene aryl sulfides **15b–e** reacted in solution exclusively at the double bond to give a mixture of the allylic hydroperoxides **16-OOH** and **18-OOH** (Figure 5 and Table 4). In all cases hydrogen abstraction occurred to a small extent preferentially at the geminal-dimethyl end of the double bond. As anticipated, the substituent on sulfur had little or no influence over the regiochemistry of the ene reaction at the remote olefinic linkage. Oxidation at sulfur competed with reaction at the double bond only in the trisubstituted alkene **15a** and in the dialkyl sulfide **15f**, presumably as a result of decreased double bond nucleophilicity and of enhanced steric access to and/or enhanced nucleophilicity of sulfur,

(48) Zhou, W.; Clennan, E. L. *Org. Lett.* **2000**, *2*, 437–440.

(49) Hiranuma, S.; Shibata, M.; Hudlicky, T. *J. Org. Chem.* **1983**, *48*, 5321–5326.

(30) Vasenkov, S.; Frei, H. In *Solid State and Surface Photochemistry*; Ramamurthy, V., Schanze, K. S., Eds.; Marcel Dekker: New York, 2000; Vol. 5, pp 295–323.

(31) Blatter, F.; Frei, H. *J. Am. Chem. Soc.* **1993**, *115*, 7501–7502.

(32) Blatter, F.; Frei, H. *J. Am. Chem. Soc.* **1994**, *116*, 1812–1820.

(33) Blatter, F.; Moreau, F.; Frei, H. *J. Phys. Chem.* **1994**, *98*, 13403–13407.

(34) Blatter, F.; Sun, H.; Frei, H. *Catal. Lett.* **1995**, *35*, 1–12.

(35) Blatter, F.; Sun, H.; Frei, H. *Chem. Eur. J.* **1996**, *2*, 385–389.

(36) Sun, H.; Blatter, F.; Frei, H. *J. Am. Chem. Soc.* **1994**, *116*, 7951–7952.

(37) Sun, H.; Blatter, F.; Frei, H. *J. Am. Chem. Soc.* **1996**, *118*, 6873–6879.

(38) Frei, H. In *Studies in Surface Science and Catalysis. 3RD World Congress on Oxidation Catalysis*; Grasselli, R. K., Oyama, S. T., Gaffney, A. M., Lyons, J. E., Eds.; Elsevier Science: New York, 1997; Vol. 110, pp 1041–1050.

(39) Myli, K. B.; Larsen, S. C.; Grassian, V. H. *Catal. Lett.* **1997**, *48*, 199–202.

(40) Vasenkov, S.; Frei, H. *J. Phys. Chem. B* **1998**, *102*, 8177–8182.

(41) Xiang, Y.; Larsen, S. C.; Grassian, V. H. *J. Am. Chem. Soc.* **1999**, *121*, 5063–5072.

(42) Blatter, F.; Sun, H.; Vasenkov, S.; Frei, H. *Catal. Today* **1998**, *41*, 297–309.

(43) Panov, A. G.; Larsen, R. G.; Totah, N. I.; Larsen, S. C.; Grassian, V. H. *J. Phys. Chem. B* **2000**, *104*, 5706–5714.

(44) Frei, H.; Blatter, F.; Sun, H. *Chemtech* **1996**, *26*, 24–30.

(45) Sun, H.; Blatter, F.; Frei, H. *Catal. Lett.* **1997**, *44*, 247–253.

(46) Vasenkov, S.; Frei, H. *J. Phys. Chem. B* **1997**, *101*, 4539–4543.

(47) Larsen, R. G.; Saladino, A. C.; Hunt, T. A.; Mann, J. E.; Xu, M.; Grassian, V. H.; Larsen, S. C. *J. Catal.* **2001**, *204*, 440–449.

TABLE 4. Photooxidations of 15a–f in Solution^{a,b}

| substrate | % conversion ^c | 15-SO | 16-OOH | 17-OOH | 18-OOH |
|------------|---------------------------|-------|--------|--------|--------|
| 15a | 47 | 14 | 46 | 40 | |
| | 64 | 18 | 42 | 40 | |
| 15b | 20 | | 55 | | 45 |
| | 62 | | 55 | | 45 |
| | 87 | | 53 | | 47 |
| 15c | 48 | | 53 | | 47 |
| 15d | 41 | | 53 | | 47 |
| 15e | 27 | | 54 | | 46 |
| 15f | 17 | 44 | 34 | 23 | |
| | 29 | 39 | 36 | 24 | |
| | 46 | 45 | 21 | 18 | |

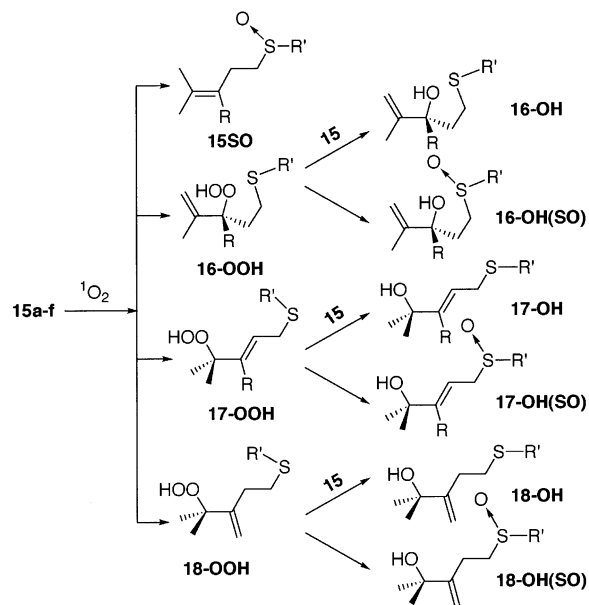
^a In CDCl₃ at room temperature using 0.1 M **15a–f** and 3 × 10⁻⁴ M tetraphenylporphyrin (TPP) as sensitizer. ^b Product ratios were measured directly by proton NMR in the photooxidation mixtures and are reproducible to ±4%. ^c To get larger % conversions the time of irradiation was extended.

respectively.⁵⁰ Hydrogen abstraction from the tether to give **17-OOH** only occurred in **15a**. The preferred 90° dihedral angle (H–CH–C=C) for hydrogen abstraction is energetically inaccessible as a result of the eclipsing interaction between the CH₂CH₂ bond of the tether and the vinyl geminal-methyl group, R, in **15b–f**. This eclipsing interaction is absent in **15a**.

The allylic hydroperoxide products were indefinitely stable in solution. Reductive decomposition, however, was enhanced by removal of the solvent. Consequently, prior to the concentration of the reaction mixtures, triphenylphosphine, PPh₃, was added to all the samples to quantitatively generate the corresponding alcohols and triphenylphosphine oxide, Ph₃PO. The different allylic alcohols and hydroperoxides could easily be distinguished by their characteristic proton NMR spectra (Experimental Section).

The intrazeolite photooxidations of **15a–f** proved to be more complex than their counterparts in homogeneous media. In addition to the sulfoxide, **15-SO**, three different allylic alcohols and their corresponding sulfoxides were also isolated from the intrazeolite photooxidation mixtures (Figure 6). Remarkably, however, in stark contrast to the homogeneous photooxidations, no allylic hydroperoxides were isolated from the reaction mixtures. This was verified by treating these reaction mixtures with PPh₃ and noting the lack of formation of Ph₃PO. The absence of allylic hydroperoxides was not due to a low mass balance, which exceed 97% in all cases, nor was it due to decomposition during workup. Control experiments demonstrated that the hydroperoxides formed in the solution photooxidation of **15a** when subjected to the same gentle acid wash and extraction procedures (see Experimental Section) survived unchanged. In addition, the proton NMR spectra of the reaction mixtures clearly demonstrated the absence of ketones or aldehydes from acid-catalyzed⁵¹ or intrazeolite cleavages³¹ of the hydroperoxides.

We suggest that the sulfide moiety, by an intrazeolite intermolecular process with a small intramolecular contribution, spontaneously reduced the allylic hydroperoxides. Experimental evidence for this suggestion was

**FIGURE 6.****TABLE 5. Product Distributions in Intrazeolite Photooxidations**

| substrate | 15a | 15b | 15c | 15f |
|------------------|------------|------------|------------|------------|
| % conversion | 26 | 30 | 26 | 40 |
| 15-SO | 73 | 57 | 53 | 68 |
| 16-OH | 13 | 19 | 10 | 14 |
| 16-OH(SO) | 14 | 10 | 18 | 9 |
| 17-OH | a | | | |
| 17-OH(SO) | a | | | |
| 18-OH | | 6 | 7 | 3 |
| 18-OH(SO) | | 8 | 12 | 6 |

^a Formed at higher conversions.

generated by adding a mixture consisting of **15a** (58%), **15a-SO** (9%), **16a-OOH** (14%), **17a-OOH** (13%), **16a-OH** (2.1%), **17a-OH** (1.7%), and several ene sulfoxides (2.9%) to a hexane slurry of NaY. This reaction mixture was then subjected to the same isolation procedure afforded the intrazeolite photooxidation mixtures. Analysis of the results by NMR demonstrated that the hydroperoxy groups are completely reduced to the alcohols in NaY in the absence of methylene blue. In addition, **15a** decreased by 9.7% concomitant with a 9.7% increase in the concentration of **15a-SO**, consistent with an intermolecular reduction pathway. The feasibility of an intermolecular pathway was also demonstrated by the oxidation of coadsorbed thioanisole. However, the inability to detect a second diastereomer corresponding to **16-OH(SO)** provides the distinct possibility that this compound may have formed via an intramolecular cyclic six-membered ring transition state.

The intrazeolite photooxidation product ratios for **15a–c** and **15f** are given in Table 5 at the lowest percent conversions convenient for analytical analysis. Overoxidation of sulfoxide **15-SO** and sulfides **16-OH**, **17-OH**, and **18-OH** is a problem at high conversion. A comparison of the data in Tables 4 and 5 reveals a remarkable increase in sulfoxide **15-SO** formation as the reaction is moved from solution into the zeolite. For example, **15a-SO** increases from 14% in solution to 73% in the zeolite.

(50) It is also possible that physical quenching, k_q in Scheme 2, competes more effectively in aryl-substituted sulfides.

(51) Porter, N. A. In *Organic Peroxides*; Ando, W., Ed.; John Wiley & Sons Ltd: New York, 1992; pp 101–156.

TABLE 6. Relative Rate Constants for Intrazeolite Reactions at Sulfur and the Double Bond as a Function of Counterion

| substrate | MY | % conversion ^b | $[k_r(\text{sulfide})]/[k_r(\text{olefin})]$ |
|------------|------------------|---------------------------|--|
| 15a | LiY ^a | 30.2 | 1.68 |
| | NaY ^a | 25.9 | 2.31 ± 0.22 |
| | KY | 36.8 | 0.65 |
| | RbY | 23.2 | 0.92 |
| | CsY | 9.5 | 0.48 |
| 15b | LiY ^a | 34.0 | 0.56 |
| | NaY ^a | 30.7 | 0.87 ± 0.10 |
| | KY | 26.1 | 0.27 |
| | RbY | 35.2 | 0.14 |
| | CsY | 21.5 | 0.04 |
| 15f | LiY ^a | 45.4 | 1.68 |
| | NaY ^a | 39.5 | 2.26 ± 0.41 |
| | KY | 36.0 | 3.08 |
| | RbY | 30.2 | 2.70 |
| | CsY | 14.8 | 1.15 |

^a These samples were only irradiated for 5 min. All other samples were irradiated for 15 min. ^b See Table S3 of the Supporting Information for product ratios.

In fact, 73% may be an underestimate, even at the modest percent conversion reported in Table 5, of the contribution of **15a-SO** to the product ratio, because of nefarious overoxidation.

A lower limit for the relative rate constants for reaction at sulfur and the olefinic linkage $[k_r(\text{sulfide})/k_r(\text{olefin})]$ can be calculated both in solution and in the interior of the zeolite for **15a** and **15f**, which give products at both sites in both media. The calculation uses the data in Tables 4 and 5 in conjunction with eq 1.⁵²

$$\frac{k_r(\text{sulfide})}{k_r(\text{olefin})} = \frac{\ln[C_o(\text{sulfide})/C_t(\text{sulfide})]}{\ln[C_o(\text{olefin})/C_t(\text{olefin})]} \quad (1)$$

The success of this approach is a direct result of the presence of the tether linking the sulfide and olefinic sites, which guarantees the close proximity of the two functional groups and as a consequence equal access to singlet oxygen. In this situation $[15]_o = C_o(\text{sulfide}) = C_o(\text{olefin})$. However, $C_t(\text{sulfide})$ must be corrected for the amount of **15-SO** formed by intermolecular reduction of the hydroperoxides in the zeolite and is therefore set equal to $[15]_o - [15\text{-SO}] + ([16\text{-OH}] + [17\text{-OH}] + [18\text{-OH}])$ for the zeolite photooxidations. The concentration of the olefin at time t , $C_t(\text{olefin})$, is set equal to $[15]_o - \Sigma[\text{ene products}]$. This treatment gives a $[k_r(\text{sulfide})/k_r(\text{olefin})]$ of 0.14 ± 0.02 and 2.31 ± 0.22 for **15a** and 0.70 ± 0.07 and 2.26 ± 0.41 for **15f** in solution and in the zeolite, respectively. These data indicate that by moving the photooxidations of **15a** and **15f** from solution to the interior of the zeolite, oxidation rate constants at sulfur are enhanced in comparison to the rate constants at the olefinic sites by factors greater than 16- and 3-fold, respectively.

The relative rate constants $[k_r(\text{sulfide})/k_r(\text{olefin})]$ were also measured as a function of counterion for the intrazeolite photooxidations of **15a**, **15b**, and **15f** (Table 6). In general, counterions generating high electrostatic fields, Na⁺ and Li⁺, show a higher propensity for reaction

(52) Higgins, R.; Foote, C. S.; Cheng, H. In *Advances in Chemistry Series*; Gould, R. F., Ed.; American Chemical Society: Washington, DC, 1968; Vol. 77, pp 102–117.

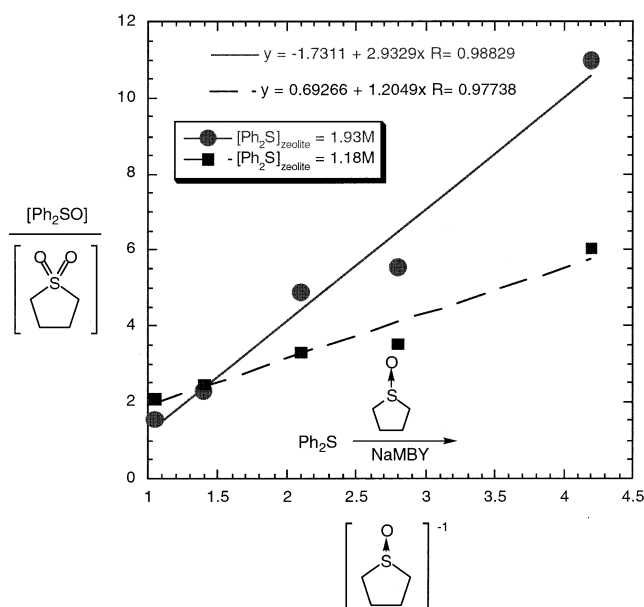


FIGURE 7. Diphenylsulfoxide/thiolane sulfone product ratio as a function of both the concentrations of Ph₂S, **11**, and thiolane sulfoxide.

at sulfur than those generating smaller electrostatic fields. This trend is very evident for aryl-substituted sulfides **15a** and **15b** but less evident for dialkyl sulfide **15f**.

To examine the possibility that an intermediate could be trapped in these experiments, the co-intrazeolite photooxidations of **11** and thiolane sulfoxide were examined. Control experiments demonstrated that thiolane sulfoxide in the absence of **11** is inert under the reaction conditions. However, coconclusion with **11** resulted in formation of thiolane sulfone, providing irrefutable evidence for an oxidatively active intermediate. A quantitative treatment of these trapping results shown in Figure 7 demonstrated that the (diphenyl sulfoxide/thiolane sulfone) ratio was a function of both the thiolane sulfoxide and **11** concentrations. This result is consistent with competitive trapping of the intermediate with thiolane sulfoxide and the substrate **11**.⁵³

Discussion

The unique features of the sulfide intrazeolite photooxidations that distinguish them from their solution counterparts include (1) an enhanced rate of reaction, (2) the ability of water to influence the sulfoxide/sulfone ratio, (3) the suppression of the Pummerer rearrangement (cleavage), (4) the ability of the substrate concentration to influence the sulfoxide/sulfone ratio, and (5) the ability of counterions to influence the efficiency of the reactions. We suggest that these unusual results can be rationalized by the mechanism shown in Scheme 3 for the intrazeolite photooxidation of diphenyl sulfide, **11**.

The key element of this new intrazeolite mechanism is the formation of a counterion complexed persulfoxide intermediate, **I**. It differs from the solution mechanism (Scheme 2) by invoking only one rather than two inter-

(53) Liang, J.-J.; Gu, C.-L.; Kacher, M. L.; Foote, C. S. *J. Am. Chem. Soc.* **1983**, *105*, 4717–4721.

counterion. In principle, the contributions of these two effects can be separated by independently measuring the rate constants for disappearance of singlet oxygen and the rate constants for product formation. If the only effect operating in the zeolite is suppression of physical quenching, the rate constant of substrate-induced singlet oxygen disappearance should be identical in solution and in the zeolite. The rate constant for disappearance of singlet oxygen can be measured in solution by following the substrate quenching of the time-resolved emission of singlet oxygen at 1270 nm.⁵⁵ Unfortunately, all our attempts to use this method to follow intrazeolite singlet oxygen decay have failed because of our inability to adequately account for the massive amounts of scattered light observed in these heterogeneous sample slurries.

If suppression of physical quenching is the only effect operating by moving these reactions into the interior of the zeolite, the relative rate constants [$k_r(\text{sulfide})/k_r(\text{olefin})$] derived from eq 1 could never exceed the ratio of solution k_T values for reaction at the sulfide and olefinic sites. These k_T ratios cannot be measured directly with the tethered substrates; however, they can be estimated using suitable monofunctionalized model substrates.^{56–58} This analysis predicts $k_T(\text{sulfide})/k_T(\text{olefin})$ values of 3.84, 0.66, 0.28, and 6.0 for **15a**, **15b**, **15c**, and **15f**, respectively. These calculated values are sufficiently close to the experimental values (2.31 ± 0.22 , 0.87 ± 0.10 , 0.70 ± 0.07 , and 2.26 ± 0.41 , for **15a**, **15b**, **15c**, and **15f**, respectively) to suggest that suppression of physical quenching has a major role, if not the exclusive role, in the ability of the zeolite to promote sulfide photooxidation.

An alternative mechanism that invokes an initiation step involving an intrazeolite-promoted electron transfer from the sulfide substrate, **11**, to singlet oxygen can be ruled out on thermodynamic grounds. The free energy for electron-transfer calculated using the Rehm–Weller equation⁵⁹ ($\Delta G^\circ = 23.06 \text{ (kcal/mol)/}V [E^\circ(\mathbf{11}/\mathbf{11}^{+\bullet}) - E^\circ(\text{O}_2/\text{O}_2^{\bullet-}) - e^2/\epsilon a] - \Delta E^\circ$) is very endothermic (29.7 kcal/mol).⁶⁰ Oxidation and reduction potentials are likely to be different in the zeolite than in solution; however, the magnitude of the change is unlikely to be sufficient to convert this endothermic process into an exothermic one.⁶¹

(55) Clennan, E. L.; Noe, L. J.; Szneler, E.; Wen, T. *J. Am. Chem. Soc.* **1990**, *112*, 5080–5085.

(56) **15a** model system: PhSCH₃, $k = 2.3 \times 10^6 \text{ M}^{-1} \text{ s}^{-1}$, and 2-methyl-2-pentene, $1.2 \times 10^6 \text{ M}^{-1} \text{ s}^{-1}$. **15b** model system: PhSCH₃ and 2,3-dimethyl-2-butene, $k = 7.0 \times 10^6 \text{ M}^{-1} \text{ s}^{-1}$. **15c** model system: pClC₆H₄SCH₃, $k = 1.0 \times 10^6 \text{ M}^{-1} \text{ s}^{-1}$, and 2,3-dimethyl-2-butene. **15f** model system: diethyl sulfide, $2 \times 10^7 \text{ M}^{-1} \text{ s}^{-1}$, and 2,3-dimethyl-2-butene. Manring, L. E.; Kanner, R. C.; Foote, C. S. *J. Am. Chem. Soc.* **1983**, *105*, 4707–4710.

(57) Monroe, B. M. *Photochem. Photobiol.* **1979**, *29*, 761–764.

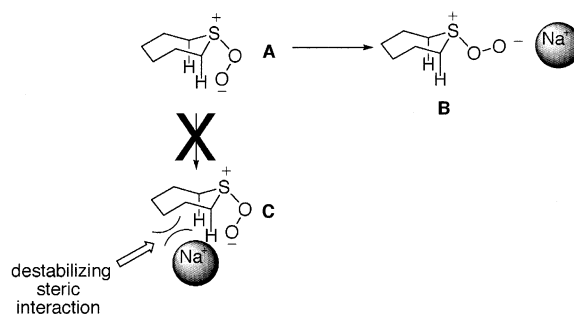
(58) Wilkinson, F. *Pure Appl. Chem.* **1997**, *69*, 851–856.

(59) Rehm, D.; Weller, A. *Isr. J. Chem.* **1970**, *8*, 259–271.

(60) The terms in the Rehm–Weller equation $E^\circ(\mathbf{11}/\mathbf{11}^{+\bullet})$, $E^\circ(\text{O}_2/\text{O}_2^{\bullet-})$, $e^2/\epsilon a$, and ΔE° represent the oxidation potential of **11** (1.483 V versus SCE in CH₃CN; Wendt, H. *Angew. Chem., Int. Ed. Engl.* **1982**, *21*, 256–270), the reduction potential of triplet oxygen (−0.82 V vs SCE in CH₃CN; Clennan, E. L.; Noe, L. J.; Szneler, E.; Wen, T. *J. Am. Chem. Soc.* **1990**, *112*, 5080–5085), the work term (0.04 V in CH₃CN) for bringing two ions to the encounter distance a in a solvent of dielectric constant ϵ , and the singlet–singlet excitation energy of oxygen (22.5 kcal/mol). The work term, $e^2/\epsilon a$, was determined from the dielectric constant for acetonitrile and the encounter distance, $a = 5 \text{ \AA}$, calculated from the radii for singlet oxygen and diphenyl sulfide.

(61) Yoon, K. B.; Kochi, J. K. *J. Am. Chem. Soc.* **1988**, *110*, 6586–6588.

SCHEME 5



The intrazeolite behavior of thiane, **5**, mimics in many respects the intrazeolite behavior observed for diphenyl sulfide, **11**. This similarity argues for analogous “single intermediate” intrazeolite mechanisms for the two substrates. The complete suppression of the Pummerer rearrangement in the five- and seven-membered ring sulfides, **4** and **6**, respectively, also lends support to this suggestion, since the second intermediate, the hydroperoxysulfonium ylide (**3** in Scheme 2), serves as a direct precursor for the Pummerer product.

The “single intermediate” mechanism depicted in Scheme 3, however, cannot be a general mechanism. In acyclic sulfides, **7**, **9**, **10**, **12**, and **13**, sulfur–carbon bond cleavage products from the Pummerer rearrangements are less important but, nevertheless, are still observed in the zeolite. These results require formation of the hydroperoxy sulfonium ylide in the zeolite. In addition, the intramolecular hydrogen-abstraction product, ethyl vinyl sulfoxide, is formed to the same extent in solution and in intrazeolite photooxidations of **14**.¹⁹ This suggests that in this case complexation of sodium to the persulfoxide cannot suppress the very rapid k_X interconversion (Scheme 2) to the extent that allows competitive trapping of the persulfoxide by the sulfide substrate (k_S in Scheme 3).

This analysis suggests that cation complexation decreases, but does not completely abolish, the negative charge on the peroxy linkage of the persulfoxide, and as a result, hydrogen abstraction (k_X in Scheme 2) is suppressed but not completely eliminated. Consequently, the complete suppression of hydroperoxy sulfonium ylide formation in the intrazeolite reactions of cyclic sulfides **4** and **6** is surprising. We suggest that in these cyclic sulfides a change in the conformation of the persulfoxide upon inclusion into the zeolite also contributes to the complete competitive inhibition of k_X . Extensive quantum chemical calculations have demonstrated that the persulfoxide adopts a bisected conformation (**A** in Scheme 5) in which the oxygen–oxygen bond bisects the carbon–sulfur–carbon bond angle.⁶² This conformation places the pendant oxygen in the persulfoxide in an ideal location to abstract an α -hydrogen to form the second intermediate. The cation complexed persulfoxide, however, will likely adopt the extended conformation **B** rather than **C** (Scheme 5) in order to minimize cation–sulfide ring interactions. Hydrogen abstraction is geometrically precluded in the thermodynamically more stable intrazeolite persulfoxide **B**. In contrast, in the acyclic sulfides greater

(62) Greer, A.; Chen, M.-F.; Jensen, F.; Clennan, E. L. *J. Am. Chem. Soc.* **1997**, *119*, 4380–4387.

conformational flexibility in the cation-complexed persulfoxide still allows adoption of the bisected conformation without severe destabilizing steric interactions.

Conclusion

We have examined the photooxidations of a series of sulfides in the interior of zeolite Y. Dramatic changes in reaction efficiency and product ratios were observed. Unfortunately, direct spectroscopic observation of intrazeolite singlet oxygen and other transient intermediates failed because of yet unsolved technical problems in this heterogeneous environment. Nevertheless, very revealing kinetic studies demonstrate that the potential energy surfaces for sulfide photooxidations are perturbed but not completely altered by moving the reaction from solution into the highly charged intrazeolite environment. The interstitial cations provide stabilization for the pivotal persulfoxide intermediates. As a consequence of this “complexation/stabilization”, the negative charge is diminished on the peroxy linkage, direct attack by the sulfide substrate is promoted, and decomposition via a physical quenching channel is inhibited. On a practical level, in comparison to their solution counterparts, the reactions are more rapid in the zeolite and the product ratios are dramatically more sensitive to traces of water.

In these photooxidations the zeolite appears to be acting as an authentic microreaction vessel. No direct (covalent) participation of the zeolite framework has been detected. However, participation of the zeolite framework has been suggested in other cases. We anticipate that as the scope of intrazeolite mechanistic studies expand, the factors that control a more active participation of the zeolite supercage will be delineated.

Experimental Section

Compounds thiolane sulfoxide, **4-SO**; thiolane sulfone, **4-SO₂**; thiane, **5**; diphenyl disulfide; thioanisole, **8**; phenyl methyl sulfoxide, **8-SO**; diphenyl sulfide, **11**; and diphenyl sulfoxide, **11SO**, were all obtained commercially and used without further purification. Thiolane, **4**, was obtained commercially and used without further purification. The compounds 4-butanol disulfide;²² thiane sulfoxide, **5-SO**;⁶³ thiane sulfone, **5-SO₂**;⁶³ hexamethylene sulfide, **6**;⁶³ hexamethylene sulfoxide, **6-SO**;⁶³ hexamethylene sulfone, **6SO₂**;⁶³ 6-hexanal disulfide;⁶⁴ phenyl allyl sulfide, **7**;⁶⁵ phenyl allyl sulfoxide, **7-SO**;⁶⁶ phenyl allyl sulfone, **7-SO₂**;⁶⁷ phenyl methyl sulfone, **8-SO₂**;⁶⁸ phenyl ethyl sulfide, **9**;⁶⁹ phenyl ethyl sulfoxide, **9-SO**;⁷⁰ phenyl ethyl sulfone, **9-SO₂**;⁷¹ phenyl isopropyl sulfide, **10**;⁷² phenyl isopropyl sulfoxide, **10-SO**;⁷³ phenyl isopropyl

sulfone, **10SO₂**;⁷⁴ diphenyl sulfone, **11-SO₂**;⁶⁹ benzyl phenyl sulfide, **12**;⁷¹ benzyl phenyl sulfoxide, **12-SO**;⁷¹ benzyl phenyl sulfone, **12-SO₂**;⁷¹ 2-phenylethyl phenyl sulfide, **13**;⁷⁵ 2-phenylethyl phenyl sulfoxide, **13-SO**;⁷⁶ 2-phenylethyl phenyl sulfone, **13-SO₂**;⁶⁸ 2-chloroethyl ethyl sulfide, **14**;¹⁹ 2-chloroethyl ethyl sulfoxide, **14-SO**;¹⁹ and ethyl vinyl sulfoxide¹⁹ are all known and their structures are consistent with their published physical data. NaY was purchased commercially and converted to NaMBY as described.

Diffuse reflectance spectra of MB-zeolites were obtained on a UV/vis/NIR spectrometer. Proton NMR spectra were obtained in CDCl₃ at 400.13 MHz and are referenced to TMS. An HP-5 [30 m × 0.25 mm × 0.25 μm (length × inside diameter × film thickness)] capillary column and a 5% diphenyl-95% dimethyl polysiloxane (30 m × 0.32 mm × 1.0 μm) fused silica column were used.

Zeolite Photolysis. The standard intrazeolite photooxidation experiment was conducted by addition of 0.3 g of dried NaMBY to 5 mL of hexane containing the substrate. This mixture was then stirred for 15 min and saturated with dry (CaCl₂) oxygen gas. These samples were then irradiated for 1 h with continuous oxygen bubbling with a 600 W tungsten-halogen lamp through a 12 M NaNO₂ 400-nm cutoff filter. After irradiation the hexane-zeolite slurry is centrifuged and the solvent decanted. The products were isolated by continuous extraction with tetrahydrofuran for 3 h or overnight using acetonitrile or methanol and analyzed by GC or in some cases by proton NMR.

Trapping Studies. The trapping studies were done using the standard photolysis protocol (vide supra) in hexane slurries using various concentrations of thiolane sulfoxide. Thiolane sulfoxide was 100% incorporated into the zeolite at all concentrations used in these studies. Using 5 mL of a 0.1 M solution of diphenyl sulfide, **11**, the intrazeolite concentration was 1.93 M, representing an average incorporation of 81% of the sulfide from solution. Using 5 mL of a 0.05 M solution of diphenyl sulfide, **11**, the intrazeolite concentration was 1.18 M, representing an average incorporation of 99% of the sulfide from solution. The concentrations were calculated using a void volume of 0.21 mL in 300 mg of the zeolite. The void volume was calculated using a value of $1.5 \times 10^4 \text{ \AA}^3$ as the volume of the unit cell and 12 700 as the molar mass of the NaY unit cell. This calculation is an approximation, since solvent does not have access into the sodalite cages and the framework also takes up volume in the unit cell. An alternative, and perhaps better, means of calculating the void volume is to use the volume of the supercage (827 Å³) and multiplying by eight supercages per unit cell. This gives a void volume of 0.095 mL in 300 mg of the zeolite and a corresponding higher concentration of thiolane sulfoxide and Ph₂S in the interior of the zeolite. This gives slopes in Figure 7 that are 2.21 times larger (0.21 mL/0.095 mL), but since the concentrations of **11** are also 2.21 times larger, this method gives the same values of k_S/k_{SO} .

Product Ratios as a Function of Substrate Loading Levels. The plots in Figure 3 were generated by adding 300 mg of dry NaMBY ($(S)_{MB} = 0.01$) to a hexane solution containing the sulfide substrate. The percent absorptions were determined by monitoring the concentration of the substrate in hexane by gas chromatography. The maximum absorption value was attained almost immediately upon addition of the zeolite to the hexane solution. The sulfoxide/sulfone ratios changed slightly as a function of percent conversion. The data in Figure 3 were generated at high conversions (27.9–98.7%; Table S1 in Supporting Information). In general, longer

(63) Block, E.; Bazzi, A. A.; Lambert, J. B.; Wharry, S. M.; Andersen, K. K.; Dittmer, D. C.; Patwardhan, B. H.; Smith, D. J. H. *J. Org. Chem.* **1980**, *45*, 4807–4810.

(64) Cox, J. M.; Owen, L. N. *J. Chem. Soc. C* **1967**, 1130–1134.

(65) Furuta, K.; Ikeda, Y.; Meguriya, N.; Ikeda, N.; Yamamoto, H. *Bull. Chem. Soc. Jpn.* **1984**, *57*, 2781–2790.

(66) Ali, M. H.; Stevens, W. C. *Synthesis* **1997**, 764–768.

(67) Schreiber, K. C. *Anal. Chem.* **1949**, *21*, 1168–1172.

(68) Pine, S. H.; Shen, G.; Bautista, J.; Sutton Jr., C.; Yamada, W.; Apodaca, L. *J. Org. Chem.* **1990**, *55*, 2234–2237.

(69) Pouchert, C. J.; Behnke, J., Eds. *The Aldrich Library of ¹³C and ¹H FT NMR Spectra*, 1st ed.; Aldrich Chemical Co.: Milwaukee, WI, 1993.

(70) Ali, M. H.; Bohnert, G. J. *Synthesis* **1998**, 1238–1240.

(71) Hepworth, H.; Clapham, H. W. *J. Chem. Soc.* **1921**, 119, 1188–1198.

(72) Iptieff, N.; Pines, H.; Friedman, B. S. *J. Am. Chem. Soc.* **1938**, *60*, 2731–2734.

(73) Barbieri, G.; Cinquini, M.; Colonna, S.; Montanari, F. *J. Chem. Soc. C* **1968**, 659.

(74) Lamothe, M.; Anderson, M. B.; Fuchs, P. L. *Synth. Commun.* **1991**, *21*, 1675–1693.

(75) Baciocchi, E.; Del Giacco, T.; Ferrero, M. L.; Rol, C.; Sebastiani, G. V. *J. Org. Chem.* **1997**, *62*, 4015–4017.

(76) Mashraqui, S. H.; Mudaliar, C. D.; Karnik, M. A. *Synth. Commun.* **1998**, *28*, 939–943.

irradiation times were needed at the higher loading levels to get comparable percent conversions. For experiments in which irradiation times of Ph₂S (**11**) and NaMBY slurries were kept constant (all 1 h), the percent conversions were very low at high loading levels and led to a lower quality linear plot.

Absorption Studies. The absorption studies depicted in Figure 2 were conducted by adding 2.5 mL of a 0.04 M hexane solution of **5** to 0.15 g of dried NaY. The amount of **5** remaining in solution was periodically analyzed by capillary column gas chromatography. The amount of **5** absorbed by the zeolite was then calculated using the following equation

$$T(\text{mmol/g}) = \{[1 - (A_t/A_{is})/(A_0/A_{is})]C_0V_0\}/W_z$$

where T = the amount of **5** absorbed per gram of zeolite, A_t = the GC area of **5** in hexane at time t , A_{is} = the GC area of internal standard (Ph₃CH), A_0 = the GC area of sulfide at $t = 0$, W_z = the weight of the zeolite in grams, C_0 = the concentration of **5** in the hexane at $t = 0$ in mmol/mL, and V_0 = the volume of the hexane (mL).

The loading level at any time t was calculated using the following equation

$$\langle S \rangle_5 = [(g_5)/(MW_5)]/(M_{\text{supercage}})^{-1}(W_z)$$

where, $\langle S \rangle_5$ = the molecules of **5** per supercage, g_5 = the grams of **5** absorbed into zeolite, MW_5 = the molecular weight of **5**, $M_{\text{supercage}}$ = the grams of dry zeolite per moles of supercage (calculated for a unit cell composition of Na₅₆(AlO₂)₅₆(SiO₂)₁₃₆ and using eight supercages per unit cell to give 1595.32 g/mol supercage).

Intrazeolite Photooxidation of 15a–f. The reaction mixtures were prepared by taking 5 mL of a hexane solution, either 0.05 or 0.1 M in **15a–f**, and adding 0.3 g of zeolite Y (occupancy $\langle S \rangle_{\text{MB}} = 0.01$; one molecule of methylene blue per

100 supercages). This hexane slurry was saturated with oxygen and stirred for 15 min and then irradiated under continuous oxygen agitation with a 600-W tungsten lamp thorough 1 cm of a 12 M NaNO₂ filter solution. The zeolite powder was then filtered and placed in a Soxhlet cup and continuously extracted overnight with chloroform. The zeolite was then mildly digested with 5 mL of 10% HCl and the mixture extracted with four 10-mL portions of chloroform. The combined organic extracts were then washed with aqueous Na₂CO₃ and dried with MgSO₄, and the solvent was removed under reduced pressure. The reaction mixtures were then characterized by proton NMR. ¹H NMR (CDCl₃): **16a-OOH** δ 5.03 (bs, 2H), 4.49 (dd, $J = 7.9, 7.8$ Hz, 1H), 3.0 (m, 2H), 1.7–2.0 (m, 2H), 1.68 (s, 3H); **17a-OOH** δ 5.70 (dt, $J = 15.7, 7.1$ Hz, 1H), 5.50 (bd, $J = 15.7$ Hz, 1H), 3.53 (dd, $J = 7.1, 1.2$ Hz, 2H), 1.21 (2, 6H); **16a-OH** δ 4.97 (s, 1H), 4.88 (s, 1H), 4.22 (t, $J = 6.1$ Hz, 1H), 3.01 (m, 2H), 1.86 (q, $J = 7.0$ Hz, 2H), 1.65 (s, 3H); **17a-OH** δ 5.62 (d, $J = 15.4$ Hz, 1H), 5.69 (dt, $J = 15.4, 6.5$ Hz, 1H), 3.51 (d, $J = 6.5$ Hz, 2H), 1.20 (s, 6H); **16b-OOH** δ 5.02 (bs, 1H), 4.98 (bs, 1H), 2.95 (m, 2H), 2.01 (m, 2H), 1.38 (s, 3H); **18b-OOH** δ 5.26 (s, 1H), 5.08 (bs, 1H), 3.18 (t, $J = 7.3$ Hz, 2H), 2.52 (t, $J = 7.1$ Hz, 2H), 1.38 (s, 6H); **16b-OH** δ 5.04 (bs, 1H), 4.90 (bs, 1H), 2.8–3.0 (m, 2H), 1.96 (m, 2H), 1.72 (bs, 3H), 1.32 (s, 3H); **18b-OH** δ 5.18 (s, 1H), 4.87 (bs, 1H), 3.10 (t, $J = 8.0$ Hz, 2H), 2.45 (t, $J = 8.0$ Hz, 2H), 1.34 (s, 3H).

Acknowledgment. We thank the National Science Foundation for their generous support of this research.

Supporting Information Available: Data for β -carotene and 2,3-dimethyl-2-butene quenching of Ph₂S oxidation, product ratios as a function of loading level, and kinetic data for **15a**, **15b**, and **15f**. This material is available free of charge via the Internet at <http://pubs.acs.org>.

JO0261808